Trends in seasonal precipitation extremes and associated temperatures along continental Chile

Miguel A. Lagos-Zúñiga (mlagosz@uchile.cl)
Center for Climate and Resilience Research https://orcid.org/0000-0002-8787-598X
Pablo A. Mendoza
Universidad de Chile Facultad de Ciencias Físicas y Matemáticas: Universidad de Chile Facultad de Ciencias Fisicas y Matematicas
Roberto Rondanelli
Universidad de Chile Facultad de Ciencias Fisicas y Matematicas
Diego Campos
Direccion Meteorologica De Chile

Research Article

Keywords: seasonal extreme precipitation, freezing level, warm precipitation, trends

Posted Date: June 27th, 2023

DOI: https://doi.org/10.21203/rs.3.rs-3040813/v1

Version of Record: A version of this preprint was published at Climate Dynamics on January 30th, 2024.
See the published version at https://doi.org/10.1007/s00382-024-07127-z.

Abstract

We characterize trends in maximum seasonal daily precipitation (seasonal Rx1day), and minimum (Tn), and maximum (Tx) daily temperatures during days with precipitation over continental Chile for the period 1970–2017, using surface stations and the AgERA5 gridded product derived from the ERA5 reanalysis dataset. We also examine seasonal trends of Sea Surface Temperature (SST), Precipitable Water (PW), Convective Available Potential Energy (CAPE), Eddy Kinetic Energy (EKE), Atmospheric Rivers (ARs) frequency, and upper air observations to seek for possible mechanisms that explain precipitation trends. Our results show an increase in precipitation extremes during fall in Northern Chile (15–30°S) and during fall and winter in Austral Chile, and mostly negative trends in Central Chile, where a few locations with positive trends are found along the coast. Although warming trends prevail for Tn (< 0.5°C/dec), cooling trends are observed in Tx during seasonal Rx1day events for almost all seasons. The highest values in Tn trends are obtained on the western slopes of the Andes. We also explore temperature scaling in surface stations, finding strong positive super Clausius Clapeyron with Tn, especially during the fall. Sounding observations in five stations across Chile, suggest warming trends at 23.5°, 33°S and 53°S, with a stabilization effect by enhanced warming in the upper troposphere, while presenting cooling trends in Puerto Montt (41.5°S). Seasonal trends in PW reveal moistening along southern-Peru and Northern-Chile during spring and summer. Positive trends in CAPE are observed over 35–40°S (austral summer and fall) and the northern altiplano (autumn). SST analyses reveal strong cooling around 30°S in winter, which may explain the negative trends in seasonal Rx1day in central Chile. A warming spot on the northern Peruvian coast during fall may be responsible for humidification in front of Northern Chile, particularly during summer and fall. Positive EKE trends are detected south of 40°S, being stronger and reaching almost all of the coast during spring. ARs frequency unveils negative trends up to -5 days/dec during summer, and positive trends of 1 day/dec in 40°- 50°S coastal regions during spring. More generally, the results presented here shed light on the main large-scale processes driving recent trends in precipitation extremes across continental Chile.

1. Introduction

Precipitation is an essential input for hydrological studies, modulating water availability and the occurrence of extreme events like floods and landslides. During the last decades, several studies have reported significant variations in extreme precipitation regimes (e.g., Trenberth, 2011, Fisher and Knutty, 2016, Fowler et al., 2021),which have been attributed to climate variability (e.g. Pei et al., 2018, Martel et al., 2018) or anthropogenic climate change (e.g. Mukherjee et al., 2018, Zou et al., 2021). Changes in extreme precipitation have been documented worldwide (Fowler et al., 2021) and have contributed to define guidelines for adaptation, risk management, and engineering design (Martel et al., 2021). Further, floods and debris flows risk analyses may benefit from characterizing possible changes in extreme precipitation events (EPEs) and associated temperatures, especially in mountainous areas, wherea future intensification of EPEs under warming conditions is expected (Fisher and Knutty, 2016).

Improved understanding of precipitation extremes is crucial for a thorough assessment of historical climate model simulations (e.g., Paxian et al., 2015; Alexander, 2016), to evaluate the realism of gridded meteorological datasets (e.g., Schumacher et al., 2020), and to examine possible relationships between warming/drier conditions and potential changes in the frequency and intensity of EPEs. Previous studies have reported a decreasing wet day fraction and more intense precipitation events with drier and warmer conditions in some regions of the United States (e.g. Jannsen et al., 2014; Prein and Meams, 2021), Europe (e.g., Zolina et al., 2008; Fisher and Knutty, 2016), Australia (e.g., Guerreiro et al., 2018), China (e.g., Zhai et al., 2005; Shi et al., 2019), India (e.g., Pal & Al-Tabbaa, 2009) and Russia (Aleshina et al., 2021). In principle, such phenomena may be connected to the Clausius-Clapeyron scaling of the water vapor with surface temperature (Fisher and Knutty, 2016; Wang et al., 2017, Guerreiro et al., 2018; Fowler et al., 2021). Nevertheless, the intensification of EPEs is not homogeneous across seasons, and negative trends have also been reported in the literature.

In South America, a few studies have examined trends in extreme precipitation, mainly through indices proposed by the Expert Team on Climate Change Detection and Indices (ETCCDI, Karl et al., 1999). Cerón et al. (2021) analyzed the trend in maximum 5-day precipitation (Rx5day) in La Plata River basin using the CHIRPS product (Funk et al., 2015), finding trends between − 20 and 20 mm/dec. More recently, Regoto et al. (2021) analyzed surface stations across Brazil, finding different spatial behavior of trends in Rx1day and Rx5day, bothshowing variations between − 30and 30 mm/dec. Cerón et al. (2022) found similar patterns with the CHIRPS product for seasonal EPE in Colombia, with an intensification up to 20 mm/dec for Rx5day events during the warm seasons.

Continental Chile (~ 17°-57°S) spans a myriad of hydroclimatic conditions, from extremely arid in the north to extremely humid in the south. According to the Köppen-Geiger climate classification, the prevailing climates in this domain are Arid, Temperate, and Polar (Sarricolea et al., 2017), influenced by the Andes Cordillera and coastal mountains, which enhance orographic precipitation (Falvey and Garreaud, 2007; Barrett et al., 2009; Garreaud et al., 2016; Massmann et al., 2017; Scaff et al., 2017; Viale et al., 2019). The Altiplano in Northern Chile (Fig. 1d) is influenced by the Bolivian High and moisture advection from the Amazonas, with precipitation events occurring during the austral summer (Vuille et al., 1999; Garreaud, 2000; Garreaud and Aceituno, 2001; Espinoza et al, 2020). Arid and hyper-arid conditions prevail on the western side of the Northern Andes, with observed mean annual precipitation varying between ~ 1 mm in Arica (18.5°S) to 85 mm in La Serena (29.5°S). Cutoff lows (COLs) strongly influence precipitation events in these latitudes, contributing up to 50% of mean annual amounts (Aceituno et al., 2021; Muñoz and Schultz, 2021) and triggering extreme events like the Atacama floods in 2015 (Barret et al., 2016; Bozkurt et al., 2016; Wilcox et al., 2016). In central Chile, most precipitation events are related to mid-latitude baroclinic perturbations and usually accompanied by atmospheric rivers (ARs), which contribute up to 40% of extreme precipitation amounts (Aceituno et al., 2021; Valenzuela and Garreaud, 2019). Although most EPEs occur during the austral winter, some events are observed during the warm season (Viale and Garreaud, 2014; Valenzuela et al., 2022), mainly associated with COLs. On the other hand, precipitation events are evenly distributed during the year in southern and Austral Chile (Aceituno et al., 2021). In general, precipitation events are strongly teleconnected with tropical modes of variability

such as the Madden-Julian Oscillation (Juliá et al., 2012; Barrett et al., 2012; Rondanelli et al., 2019), the Pacific Decadal Oscillation, and the El Niño Southern Oscillation (Garreaud, 2009; Schumacher et al., 2020; Aceituno et al., 2021).

To the best of our knowledge, no previous studies have characterized seasonal trends in extreme daily precipitation and associated temperatures in Chile. Further, only a few studies have examined trends in precipitation and temperature across continental Chile, focusing on climatological aspects such as mean annual temperature (e.g. Falvey and Garreaud, 2009) and mean annual precipitation (e.g., Boisier et al., 2016), or other metrics such as precipitation concentration (Sarricolea et al., 2019) and aggressiveness (Valdés-Pineda et al., 2016). Souvignet et al. (2012) focused on northern Chile (29–32°S), finding a positive trend in Rx5days over the Andean region (< 10 mm/dec), with no clear spatial patterns in other climate change ETCCDI indices. Valdes-Pineda et al. (2016) showed positive, weak (i.e., not statistically significant) trends in annual precipitation (36–44°S), finding significant, positive trends north to 42°S during the period 1996–2006 and some negative trends to the south; nevertheless, they found fewer stations with significant trends when considering a longer time-window (1914–2006). Boisier et al. (2016) reported regional drying conditions for annual precipitation (-65 mm/dec) in central-southern Chile (30–40°S) from 1979 to 2014. More recently, Schumacher et al. (2020) reported positive trends in summer precipitation north of 26°S and negative trends in austral winter precipitation (26–35°S) in the period 1985–2015.

In terms of temperature, Falvey and Garreaud (2009) reported positive trends in mean annual values on valley and mountain stations (0.25°C/dec) and coastal cooling (-0.2°C/dec) with surface observations within the period 1979–2006. Positive trends have generally been detected for northern Chile's maximum and minimum temperatures (~ 0.46°C/dec, Souvignet et al., 2012). Schumacher et al. (2020) found generally warmer conditions between 15–40°S, without clear signals of change in extreme temperatures. These warming trends have induced an upward trend in the snow line elevation of 10–30 m/year south of 29–30°S (Saavedra et al., 2018).

Previous studies analyzed the mechanisms driving wintertime EPEs in central Chile considering: (i) the relationship between water vapor transport at different pressure levels (e.g., Falvey and Garreaud, 2007), (ii) the role of the Andes in orographic precipitation (e.g., Barret et al., 2009; Garreaud et al., 2019, Massmann et al., 2017), and (iii) Integrated Vapor Transport (IVT) and its role on EPEs (Valenzuela and Garreaud, 2019) and landslides (Rutllant et al, 2023). Hence, summer precipitation events have received less attention because they contribute less than 10% of annual precipitation (Viale and Garreaud, 2014). Nevertheless, these events have triggered severe floods and/or debris flows, with economic damages and fatalities in the Arid Atacama region (Bozkurt et al., 2016; Rondanelli et al., 2019), the Austral Santa Lucía village (Somos-Valenzuela et al., 2020) and Central Chile (Valenzuela et al., 2022) due to a rise in rainfall contributing area and humidity, leading to higher storm intensity. Additionally, regional and global projections indicate an increase in EPEs for Northern Chile (Ortega et al., 2019) with higher freezing levels (Mardones and Garreaud, 2020) and generally drier and warmer climatic conditions (Araya-Osses et al.,

2020; Vicuña et al., 2021). Given these conditions, understanding seasonal changes in precipitation and associated temperature become critical for the region.

This paper aims to detect and characterize trends in seasonal maximum daily precipitation and study their thermal characteristics including freezing level behavior across continental Chile, analyzing temperature and Clausius-Clapeyron scaling. Specifically, we examine surface meteorological observations and upper air sounding data during the 1973–2017 period. We also explore climatological trends in precipitable water (PW), instability, Sea Surface Temperature (SST), Eddy Kinetic Energy (EKE), and Atmospheric Rivers frequency to discuss possible mechanisms that explain some of the detected trends.

2. Data

Precipitation (Pr), maximum (Tx), and minimum (Tn) daily temperature data for the period 1970–2017 were obtained from meteorological stations (Fig. 1b,c) managed by the Chilean Water Service (*Dirección General de Aguas*, DGA) and the National Weather Service (*Dirección Meteorológica de Chile*, DMC), retrieved from the climate explorer service (CR2, 2020). These observations are not homogeneously distributed across continental Chile and are mainly concentrated below 2000 m a.s.l. (Fig. 1d-g), with more records of Pr (405 stations, Fig. 1b) than extreme temperatures (129 stations, Fig. 1c). Standard quality control (QC) procedures were performed on meteorological surface station data, including: (i) precipitation records outside seven standard deviations from the climatological mean were flagged as missing; (ii) exclusion of stations with more than two years of gaps, and (iii) removal of records with Tn > Tx. A station was flagged as complete if it had more than 98% of days with records (~ 90 days per season), and trends were computed for stations with more than 25 years of records.

We also used records of temperature, freezing level elevation (H_0, 0° isotherm), and PW from five upper air stations (Table 1, Fig. 1a). To analyze stability trends, we computed surface convective available potential energy (CAPE), which can be used as a proxy for the maximum updraft strength within a thunderstorm, and the convective inhibition (CIN) used as a proxy for near surface stability. All radiosonde variables were observed at 12 UTC (8 hours local time) on the same day of maximum daily seasonal precipitation per year, hereafter referred to as seasonal Rx1day.

We discarded sounding days with short records of thermodynamic variables required to compute CAPE/CIN and PW – defining a minimum pressure level of 500 hPa. We truncated observations up to 10 km. a. s. l., and obtained the freezing level by linearly interpolating these observations along the vertical, after finding the first record with a temperature below 0º C. If the observed surface temperature was < 0º C and positive at higher tropospheric levels, the H_0 was computed considering the second negative observation from the surface. CAPE/CIN and PW were obtained using the MetPy Python library (May et al., 2021).

Table 1
Radiosonde stations analyzed in this study.

Radiosonde station	WMO code	Latitude	Longitude	Elevation [m a.s.l]	Observational Period
Cerro Moreno Antofagasta	85442	-23.45	-70.44	115	22/01/1973–31/12/2017
Quintero	85543	-32.79	-71.53	13	10/01/1973–31/12/1999
Santo Domingo	85586	-33.64	-71.61	77	24/12/1999–31/12/2017
El Tepual Puerto Montt	85799	-41.45	-73.08	87	26/01/1973–31/12/2017
Carlos Ibañez Punta Arenas	85934	-53.00	-70.85	36	22/07/1976–31/12/2017

Since upper air observational technologies have experienced considerable changes (Elliott and Gaffen, 1991; Ross and Gaffen, 1998), and, therefore, it was unfeasible to compute seasonal trends. We considered a year with more than 182 days of records as complete, removing records greater than five standard deviations for each variable within a specific pressure level. The number of sounding profiles in Punta Arenas was much smaller than in other stations and, therefore, we relaxed the criteria to a minimum of 90 days of observations to consider a year as complete (*See Figures S1 to S5*).

We also used PW, CAPE, and CIN from the ERA5 reanalysis (Hersbach et al., 2020) at 12 UTC to emulate the observational time at the sounding stations; SSTs retrieved from the extended NOAA reconstructed SST v5 (Huang et al., 2017); and Pr from the agrometeorological product derived from hourly surface ERA5 product, hereafter, AgERA5 This product was aggregated to daily time steps and corrected using a finer topography at a 0.1° horizontal resolution (Boogard et al., 2020). Here we do not show the results of Tx and Tn during seasonal Rx1day trends, as the spatial correlation between observations and simulations was weak and for some seasons, negative (not shown).

3. Methodology

3.1. Trend detection

Seasonal trend analyses were performed separately over austral (i) summer (DJA), fall (MAM), winter (JJA), and spring (SON) Rx1day time series derived from meteorological stations; (ii) associated Tx and Tn; and (iii) observed PW, H_0 and air temperature from the radiosonde station closest to a Pr surface station. The magnitude and statistical significance of detected trends were quantified through the Sen's slope estimator (Sen, 1968), and the Mann-Kendall test (Mann, 1945; Kendall, 1948), respectively implemented in the Matlab package *Taub* (Burkey, 2021). A trend was considered statistically significant

if the p-value was < 0.1, i.e., 90% of interval confidence. We repeated these analyses using the AgERA5 for comparative purposes, and computed the Spearman rank correlation coefficient between AgERA5 and station-based trends.

In the case of Tx and Tn trends (dT/dt), we also computed the altitudinal change of temperature (dH/dt) with *Eq. 3.1* to compare against the variation of $H_0 (dH_0/dt)$ obtained with the soundings:

$$\frac{dH}{dt} \approx \frac{1}{\gamma}\frac{dT}{dt} \qquad (3.1)$$

In Eq. 3.1, we considered a standard lapse rate of $\gamma \approx -6.5^{\circ}C/km$.

To examine possible connections between physical mechanisms and the detected trends, we analyzed trends in seasonally-averaged values of PW and CAPE – retrieved from ERA5 (Hersbach et al., 2020), and reconstructed SST time series (Huang et al., 2017). Additionally, we computed trends in the storm track activity and atmospheric river frequency to examine the role of synoptic-scale precipitation systems in the long-term trends in seasonal Rx1day and associated Tx and Tn.

As a measure of storm track activity, we calculated the vertically-averaged eddy kinetic energy (EKE, Eq. 3.2) using daily 12UTC data from ERA-5 reanalysis from 850 hPa to 500 hPa, with a ten-day high-pass filter for the Southern Hemisphere (e.g., Shaw et al., 2016),

$$EKE = \frac{1}{2}\overline{(u' + v')}, \qquad (3.2)$$

where $u\prime$ and $v\prime$ denote the high-frequency fluctuation of winds, i.e., daily differences from the mean wind. For the AR frequency, we used the AR catalog from Guan and Waliser (2015) derived from ERA-Interim data. Seasonal trends and associated statistical significance were also computed through the Sen's Slope and Mann-Kendall tests.

3.2. Temperature scaling

The Clausius-Clapeyron equation states that the saturation vapor pressure in the atmosphere increases with temperature at a rate of ~ 7%/°C, and has been used to compare against observed and modeled trends in extreme precipitation under a warming world scenario (e.g., Fischer and Knutti, 2016). The CC scaling can be computed with different approaches including binning temperatures, considering hourly extreme precipitation, hourly and daily temperature, or dew-point temperature (Martinkova and Kysely 2020). Since the binning temperature approach led to high variability in the results for our study region (not shown), we decided to report scaling results with all the events by season fitting a linear regression between the non dimensional seasonal Rx1day predictand (y_{season}, *Eq. 3.3*, where t denote a year) and observed predictors (Tx and Tn) for at least 15 years by season, considering a 90% confidence level:

$$y(t)_{season} = Rx1day(t)_{season}/\underline{Rx1day_{season}} \quad (3.3)$$

3.3. Radiosonde variations

Radiosonde measurements of PW, CAPE, CIN, and H_0 were also analyzed to detect changes in 21-year averages at each station across wet (Pr > 0 mm) and dry days, using the Wilcoxon rank-sum test (Wilcoxon, 1992). Santo Domingo and Quintero are compared to each other referentially since they are ~ 95 km apart. As an example, in Antofagasta the compared periods are 1973–1995 and 1996–2017.

To detect air temperature trends, we computed the Sen's slope to interpolated averaged values between 1000 [hPa] to 100 [hPa], every 50 hPa, during wet and dry days. To compute trends, we considered complete soundings reaching at least 500 hPa (~ 5600 m a.s.l.). The completeness of records per year, pressure level, and years considered for trend calculation for each radiosonde station is shown in *Figure S6.*

4. Results

4.1. Precipitation trends

Stations with significant positive trends were found for all seasonal Rx1day time series, with the largest magnitudes (> 4 mm/dec) obtained for fall (MAM) in northern Chile (Fig. 2b). Conversely, spring Rx1day (Fig. 2d) exhibits the strongest negative trends in central and southern Chile (< -22 mm/dec). Interestingly, the fall and spring Rx1daytime series yield up to 33% of stations with significant trends. The Austral region (south of 50°S) exhibits generally positive trends in Rx1day for all seasons (Fig. 2). The AgERA5 product provides similar spatial patterns in Rx1day trends for all seasons (Fig. 2e-h), except summer events in Central Chile – for which positive trends were detected with AgERA5 (Fig. 2e). Figure 2 reveals a weak correlation between observed and simulated trends in seasonal Rx1day (except for fall and spring) across continental Chile, with a few locations with opposite signals (i.e., different sign of the trends between observations and AgERA5 product) mainly concentrated in South and Austral Chile (Fig. 2i-l).

Figure 3 displays Rx1dayS trends as a function of distance from the coast and elevation. The results show an increase of seasonal Rx1day in almost all seasons for inland high elevated stations located in the Austral region. In northern Chile, trends are significantly correlated with elevation during the warm seasons, (ρ < -0.75, *Figure S7a,c*), with negative trends for stations above ~ 3500 [m a.s.l.] (Fig. 3e); additionally, trends are negatively correlated with distance from the coast during fall (ρ = -0.57). In Central Chile, negative relationships with inland distance and altitude are generally observed during winter and spring, with most stations holding negative trends (Fig. 3c,d,g,h). Statistically significant correlations with elevation were also found during fall in this region, where an intensification in seasonal Rx1day was detected in stations above 1000 [m a.s.l] (*Figure S7c*). In southern Chile, generally negative correlations

between trends and the two variables (i.e., elevation and distance to the coast) are found in all seasons, with inland (and higher) stations providing the most negative significant trends (*Figure S7a,c*). When all stations are considered (i.e., stations with significant and non-significant trends), observed trends are positively correlated with elevation during the warm season south of 40°S and Central Chile (*Figure S7d*).

4.2. Temperature trends for seasonal Rx1day events

The trend analysis over Tn during seasonal Rx1day events reveals generally warming conditions in north and austral regions, and cooling along the coast and valleys of central and southern Chile (Fig. 4a-d). This cooling pattern expands equatorward and poleward during spring, covering the region between 24°S and 39°S (Fig. 4d). Using a standard lapse rate, the observed Tn trends during seasonal Rx1day (AgERA5) can be approximated to trends in isotherms ranging from − 800 m/dec to 800 m/dec (-1.5 to 1.5 km/dec). Interestingly, a very different behavior of Tx trends (compared to Tn) during seasonal maximum daily precipitation events was obtained regarding signal and spatial distribution (Fig. 4e-h). Although austral fall (MAM) is a warm season across continental Chile, local cooling is observed at some stations of the North, Central, and Austral regions for Tx (Fig. 4f). Further, a clear cooling signal in Tx during seasonal Rx1day is observed north of 42°S during spring (Fig. 4h).

Figure 5 shows Tn trends during seasonal Rx1day events as a function of distance from the coast and elevation. Generally, warming conditions in all regions and seasons are obtained for inland elevated stations, and cooling behavior is detected for some coastal gauges. Further, it is evident that the magnitude of warming trends increases with elevation and distance from the coast in northern Chile (Fig. 5), with a Spearman correlation coefficient between 0.53 and 0.89 (*Figure S8*). Indeed, the strongest positive correlation between trends and elevation was found for the fall season in that subdomain, which is maintained when considering the trends in all stations (regardless of their significance, *Figure S8c*). The Austral region exhibits positive statistically significant correlation between Tn trend and distance from the coast in spring ($\rho = 0.64$). Similar results for Tx are presented in the supplementary material (*Figure S9*).

4.3. Temperature scaling

The results in Fig. 6 show that seasonal Rx1day scales positively with Tn for most regions and seasons except spring, when negative scaling occurs between 24° and 33°S (Fig. 6d). During winter, sensitivities are similar to the CC scaling (~ 7%/°C) in central Chile; however, larger sensitivities (also known as super-CC, e.g., Lenderink et al., 2011) are observed north of 30°S, where other physical processes dominate, such as COLs and deep convection, contributing to the formation of convective, short-duration precipitation events (Trenberth, 2011; Loriaux et al., 2013; Lenderink et al., 2017; Fowler et al., 2021). In northern and central Chile, we found negative scaling between seasonal Rx1day and associated Tx (*Figure S10,a-d*), which has been explained by Lenderik et al., (2011) and Molnar et al. (2015) for the constraining of vapor availability for precipitation in arid conditions during these events, however, this must be verified.

4.4. Variations in radiosonde thermodynamic variables during seasonal Rx1day events.

We examined possible temporal variations in H_0, PW, CAPE, and CIN during wet (Pr > 1 mm) and dry days (Fig. 7), considering two consecutive climatological periods (each with the same length). The results show more precipitable water in Antofagasta (1.6 mm on wet days, Fig. 7, Table 2) in comparison to the first period (1973–1995), but the interquartile distribution of PW is very similar for the rest of the stations and periods on wet and dry days. Additionally, a pronounced increase in H0 during wet days has been observed in Antofagasta (~ 150 m median, 500 m for the first quartile), while no clear changes are detected for the remaining sounding stations if data is stratified into wet and dry days. The results in Table 2 reveal a clear trend towards more convective inhibition in all stations during dry days, a decrease in CAPE at Antofagasta, Quintero/Santo Domingo and Punta Arenas, and less PW (< 2 mm) during dry days. Finally, a significantly lower freezing level (~-108 m) for all days is detected in Punta Arenas compared to the 1976–1996 period. During seasonal Rx1day events, additional trends were calculated for H0 and PW. However, no definitive conclusions could be drawn due to the lack of statistical significance, except for Quintero during fall and spring up to 3.5 mm/dec (see Table S4, Figure S11).

Table 2: Changes in mean upper air sounding observations for the Wilcoxon rank-sum test, computed as the differences between 1997-2017 and 1976-1996 averages. The numbers in parentheses show the p-values of the test. Red (blue) indicates statistically significant negative (positive) trends.

Change in Variable		Antofagasta	Quintero/ Santo Domingo	Puerto Montt	Punta Arenas
PW [mm]	Wet days	1.6 (0.723)	-1.4 (0.002)	-0.2 (0.296)	-0.7 (0)
	Dry days	-1.8 (0)	-1.3 (0)	-0.1 (0.999)	-0.5 (0)
CAPE [J Kg^{-1}]	Wet days	-5.2 (0.296)	-40.7 (0)	-11.0 (0.684)	-5.1 (0.040)
	Dry days	-21.8 (0.002)	-24.4 (0)	-14.9 (0.488)	-8.1 (0)
CIN [J Kg^{-1}]	Wet days	-27.0 (0.188)	27.4 (0.003)	5.7 (0.512)	2.3 (0.059)
	Dry days	12.6 (0)	9.0 (0)	12.3 (0.008)	5.9 (0.027)
H0 [m]	Wet days	262.3 (0.228)	-25.1 (0.433)	18.1 (0.575)	-108.3 (0)
	Dry days	194.3 (0)	42.9 (0.101)	-62.1 (0.133)	-15.1 (0.039)

The trends in upper air temperatures reveal an instability trend during dry days at Quintero due to surface warming (up to 0.5°C/dec in Quintero between 900 and 800 hPa), and low-level cooling (>-0.5°C/dec) during the period 1973–1999 (Fig. 8b). Santo Domingo station showed a stabilization condition due to warming during dry and wet days in the upper troposphere (Fig. 8c). In Punta Arenas, enhanced warming in low levels (600 – 500 hPa) was detected, in comparison to cooling trends near the surface. However, as fewer observations were available in Punta Arenas, these trends do not necessarily represent the

analyzed period. Enhanced warming at mid-levels (600 – 500 hPa, compared to the surface) was found in Antofagasta (Fig. 8a), conversely statistically significant cooling was detected in Puerto Montt during dry days (Fig. 8f). The surface temperature trend at the nearest meteorological station from radiosonde (triangles in Fig. 8) did not match the magnitude of the lowest level trend estimated by radiosonde, except in Santo Domingo and Puerto Montt (Fig. 8c,d). This results are in agreement with the annual trends reported by Burger et al. (2018).

5. Discussion

5.1. Trends and scaling relationships

The results presented here unveil three main features of seasonal Rx1day in Chile: i) positive trends in summer Rx1day events over the Chilean Altiplano and fall events across 25–30°S; ii) negative trends (i.e., drying) in almost all seasons across central and southern Chile; and iii) intensification in almost all seasons across the Austral region. These patterns align well with previous studies (Souvignet, 2012; Schumacher et al., 2020), and some of them are well captured by the AgERA5 product, especially during fall and spring ($r > 0.45$, Fig. 2).

We found a strong relationship between Tn trend magnitudes and elevation in Northern Chile (Austral Chile) for all seasons (fall), in agreement with previous work in mountain regions (e.g., Pepin and Lundquist, 2008; Souvignet et al., 2012; Chimborazo et al. 2022; Pepin et al., 2022) and with Falvey and Garreaud (2009), who also detected the regional coastal cooling trends reported here. The results show a more random behavior in Tx trends, with positive correlations with elevation and distance to the coast, mainly in northern Chile.

The strongest temperature scaling to enhanced seasonal Rx1day was found for the fall season in most of the territory (18%/°C on average). The nearest CC scaling (i.e., ~ 7%/°C) was found in the austral region and super CC scaling in northern Chile, where precipitation mechanisms are mostly associated with synoptic activity and the storm track for the Austral region, and convective activity in the Altiplano. The positive scaling during the convective precipitation events aligns well with previous studies on similar precipitation-genesis regions (Hadwick et al., 2010; Lendeink et al., 2017; Mukherjee et al., 2018; Guerreiro et al., 2018; Aleshina et al., 2021; Fowler et al., 2021).

5.2. Possible mechanisms

To seek reasons behind the observational trends detected in continental Chile, we looked for climatological trends in seasonal PW and CAPE simulated by the ERA5 reanalysis over the 1979–2017 period. The results for PW indicate an increase in summer and fall moisture along the Pacific coast north from 30°S and drying trends in most continental Chile for all seasons, with the largest magnitudes (~-1 mm/dec) between 25–35°S (Fig. 9a-d). The atmospheric drying south of 30°S aligns well with the observed poleward expansion of the Hadley circulation Cell (e.g., Hu and Fu, 2007; Hu et al., 2011); additionally, the subsidence zone has shifted to subtropics and, consequently, dryer conditions have been

observed, aligning well with projected climate change impacts (He and Soden, 2016). The negative trends in PW across continental Chile agree with those detected in seasonal Rx1day, while the positive trend in the north Pacific Coast may explain the positive trends detected with observations and the AgERA5 product during the fall season (Fig. 2). Inconsistencies between observed trends in PW and ERA5 might be explained by the spatial representativeness of observations (probably more representative of inland sites) and changes in measurement techniques and radiosonde technologies (Elliott and Gaffen, 1991); in particular, the latter, overestimated water vapor before 1987, especially in dry regions as Antofagasta (Ross and Gaffen, 1998).

The trend analysis of CAPE (Fig. 9e-h) reveals an intensification of convective instability on the Pacific coast north from 35°S, which could trigger more convective precipitation over the continent. During fall, strong positive trends in CAPE are detected over the Altiplano and positive trends over the northern coast and the western Andes between 35–42°S, up to 5 [JKg^{-1}/dec], during summer and fall (Fig. 9e,f). Negative trends of CAPE north of 40°S may contribute to explain the detected trends in winter and spring Rx1day in continental Chile (Fig. 9g,h), in agreement with Taszarek et al., (2021), strengthening the effect of the subsidence intensification in the subtropics and the expansion of the Hadley Cell (He and Soden, 2016; Hu and Fu, 2011). In general, very few of the historical soundings at 12 UTC (8 Chilean local time) has surface CAPE nor CIN, probably due to the lack of buoyant energy at that time, so no general conclusions could be drawn.

If the CAPE trends detected for the warm season project for the next decades along with increasing PW, serious socio-economic damages are expected due to more intense precipitation events during summer or fall, which may trigger landslides and floods (Viale and Garreaud, 2014; Bozkurt et al. 2016, Somos-Valenzuela et al., 2020). Hence, infrastructure design and adaptation strategies should be revisited considering climate change projections for this domain (Vicuña et al., 2021), which are expected to impact the precipitation phase with higher freezing levels (Mardones and Garreaud, 2020) and, therefore, larger rainfall volumes (e.g., Lagos and Vargas, 2014; Ortega et al., 2019). Another interesting feature is the intensification of CAPE during fall between 34ºS and 40ºS during the tornado season in southern Chile (Vicencio et al., 2021), which may lead to an increased frequency of these events.

The trend analysis of SST during the period 1979–2017 (Fig. 10) reveals a hot spot in the Western Pacific (20–40°S, 170 – 140°W), previously reported by Garreaud et al. (2021), and a cooling zone near the Peruvian coast, more pronounced during winter and spring. The results also show a statistically significant cooling trend in SST south of 60°S, reflecting the lower surface pressures, and the intensification of the storm track (Chemke et al., 2022), these results align with EKE positive trends (Fig. 11a-d) that explain positive seasonal Rx1day trends during Fall and Winter in the Austral region (Fig. 2). Finally, the warming trend of fall SST in the El Niño 3.4 region may contribute to the observed intensification of seasonal Rx1day for the same season across North and Central Chile, in agreement with previously reported teleconnections (e.g., Garreaud, 2009; Aceituno et al., 2021) and their implications on extreme events (e.g., Bozkurt et al., 2016).

The EKE trends (Fig. 11a-d) reflect weaker or no eddy activity trends between 30–40°S during summer, fall, and winter. Nevertheless, strong EKE trends appeared in the Austral region, reflecting the intensification of waves and storm tracks in these latitudes, which may explain the positive trends in Rx1day events for all seasons. The AR trends only showed an intensification in frequency up to 2 days/dec during spring (Fig. 11h), but less AR days between summer and winter south of 35°S, in agreement with Ma et al. (2020). The joint decrease of ARs, and EKE in mid latitudes, may explain the negative observed trends in extreme precipitation events along central and southern Chile.

Based on the above evidence, we hypothesize that the following mechanisms may explain the observed shifts in extreme seasonal precipitation across Chile.

I. The intensification of northern summer Rx1day events may be associated with higher SST and more water vapor supply on the Pacific coast, favoring stronger precipitation.
II. The negative trends in seasonal Rx1day in central Chile could be explained by the combination of the Hadley Cell expansion (Hu and Fu, 2011) and the Southern Blob (Garreaud et al., 2021), which contribute to drier conditions (i.e., less PW) in the Pacific coast between fall and spring, in addition to the negative trends in ARs frequency.
III. The intensification in seasonal Rx1day across the southern and Austral regions can be associated with the South Pacific Pressure trend dipole and its impacts on the southern hemisphere storm track (Chemke et al., 2022), observed in the EKE trends, which may have stronger impacts on extreme precipitation than the detected instability inhibition in this region.

5.3. Limitations and future work

In this work, we did not address possible uncertainties in high-elevation observation due to precipitation undercatch. Most rain gauges installed along the Chilean Andes are conventional and lack windshields, despite the exposure to high wind speeds. Although the bias correction factor has been estimated to vary between 1.2 and 3 (Beck et al., 2020), we did not correct observed precipitation data due to the lack of in-situ temperature observations in all Pr stations. Hence, the intensification of seasonal Rx1day with elevation detected here could be attributed to measurement artifacts, i.e., warmer temperatures allowing the current weather network to measure total precipitation amounts that decades ago could not be captured due to their phase (i.e., snowfall). Additionally, a more reliable gridded meteorological product is needed to generalize the detected trends in temperatures during seasonal Rx1day. Even the station-based gridded product CR2METv2.5 (Boisier et al., 2018; DGA, 2017; Álvarez-Garretón et al., 2018) did not show better performance in temperature trends than AgERA5 during seasonal Rx1day (not shown), which remains a challenging issue in the Andes.

Further analyses are needed for temperatures associated with seasonal Rx1day, and the results presented here are not generalizable to all regions due to the weak and sometimes even negative correlations between observations and the AgERA5 product (not shown). In this context, the hypothesis of enhanced warming in mountain areas is only representative of northern Chile and is not generalizable to all the data

analyzed (as higher latitudes), as reported by Pepin et al. (2022). To draw more robust conclusions regarding temperature influence in EPEs, more stations and longer records are needed in conjunction with more humidity observations to analyze Clausius-Clapeyron relationships and sub-daily records in precipitation stations.

Our CC scaling approach is not comparable with other studies due to the small number of events considered per station (~ 30 events/season), which provided very sensitive (and even contradictory) shifts in the signal change (i.e., from positive to negative and vice versa), depending on the number of bins and extreme daily temperature selected. Further, most regional studies aggregate significant events and stations within a domain (e.g., Lenderink et al., 2017; Fowler et al., 2021). Because of the above reasons, our scaling results should be interpreted with caution; for example, the combination of coastal cooling and drying signal in central Chile led to a strong positive Tn scaling that could be misinterpreted as seasonal Rx1day intensification in the context of an expected future warming signal (Araya-Osses et al., 2020; Vicuña et al., 2021; Lagos-Zúñiga et al., 2022), contradicting the observed negative trends in that region.

6. Conclusions

We have examined trends in seasonal precipitation extremes over continental Chile and their associated maximum and minimum daily temperatures. Although statistically significant trends (90% of confidence) were detected in only 12% of the stations analyzed, we found clear patterns of intensification in precipitation extremes in Northern Chile during austral summer, and between 25–30°S during fall, followed by less intense seasonal daily maximum precipitation in central-southern Chile. Additionally, we detected an intensification of seasonal Rx1day for the Austral region in almost all seasons. Most of these spatial trends were also detected using the AgERA5 product during all seasons (p-value < 0.05). The strongest trends are ~ 4 mm/dec in the Altiplano (summer) and around 30°S during fall, while the most negative signals were found at ~ 38°S for almost all seasons (< − 4 mm/dec).

Consistently higher Tn values were detected during extreme seasonal precipitation events. Such trends are positively correlated with terrain elevation through all seasons in Northern Chile (< 0.5°C/dec), in agreement with trends reported for mountainous areas across the globe. Despite generally negative trends for Tx were detected during the warm seasons and austral winter, positive trends were found in high-elevation stations, which may lead to increased runoff contributing areas due to higher freezing levels (trends up to 800 m/dec). Because of the orographic enhancement, a possible increase in extreme flood and debris flow events in watersheds adjacent to the Andes should be explored.

We found positive trends in precipitable water in the Northeastern Pacific and negative trends around central Chile. The latter may be associated with the poleward shift of the Hadley Cell, the South Pacific Trend Dipole, the Southern Blob, and less frequent Atmospheric Rivers reaching these latitudes. These mechanisms not only affect annual precipitation, but also extreme events. We found an intensification of sea surface temperature near the coast of Peru, which may be triggering the humidification of the

northern Pacific coast of Chile during the warm seasons. The positive trends in seasonal Rx1day in Southern and Austral Chile can be attributed to the observed intensification of the southern storm track (reflected in the intensification of Eddy Kinetic Energy activity and related synoptic-scale phenomena), but also to greater atmospheric instability and more water vapor available due to generally warmer conditions.

Although no significant trends were detected for CAPE and CIN from radiosondes, we found climatological variations in the frequency and a trend towards a more unstable atmosphere in Quintero and Puerto Montt during wet days (Pr > 0 mm), but the overall trend is towards a more stable atmosphere due to warmer trends in high levels compared to the surface during dry days. Nevertheless, the ERA5 reanalysis reveals an intensification of CAPE during summer and fall in Southern Chile, the Bolivian Altiplano and high-elevated areas in the Central Andes (summer). The latter effect should be investigated in detail because of the risk in convective precipitation events and their consequences on flooding and landslides observed worldwide.

Declarations

Funding

Miguel Lagos-Zúñiga has been supported by the Chilean ANID Doctoral grant N° 21192178. Pablo A. Mendoza received support from Fondecyt Project 11200142. Miguel Lagos-Zúñiga and Pablo A. Mendoza acknowledge CONICYT/PIA Project AFB220002. Miguel Lagos-Zúñiga and Roberto Rondanelli received support from FONDAP/ANID Project 1522A0001.

Competing Interests

The authors have no relevant financial or non-financial interests to disclose.

Author Contributions

All authors contributed to the study's conception and design. Material preparation, data collection, and analysis were performed as follows: Miguel Lagos-Zúñiga wrote the first draft of the manuscript, and the other authors contributed scientific discussion, revision and preparation of the previous versions. All authors read and approved the final manuscript.

Data Availability

The datasets used during and/or analyzed during the current study are available in public repositories and referenced in the manuscript.

References

1. Aceituno P, Boisier JP, Garreaud R, Rondanelli R, Rutllant JA (2021) Climate and Weather in Chile. Water Resources of Chile. Springer, Cham, pp 7–29
2. Aleshina MA, Semenov VA, Chernokulsky AV (2021) A link between surface air temperature and extreme precipitation over Russia from station and reanalysis data. Environ Res Lett 16:105004. https://doi.org/10.1088/1748-9326/ac1cba
3. Alexander LV (2016) Global observed long-term changes in temperature and precipitation extremes: A review of progress and limitations in IPCC assessments and beyond. Weather and Climate Extremes 11:4–16. https://doi.org/10.1016/j.wace.2015.10.007
4. Alvarez-Garreton C, Mendoza PA, Boisier JP, Addor N, Galleguillos M, Zambrano-Bigiarini M, …, Ayala A (2018) The CAMELS-CL dataset: catchment attributes and meteorology for large sample studies–Chile dataset. Hydrol Earth Syst Sci 22(11):5817–5846. https://doi.org/10.5194/hess-22-5817-2018
5. Araya-Osses D, Casanueva A, Román-Figueroa C, Uribe JM, Paneque M (2020) Climate change projections of temperature and precipitation in Chile based on statistical downscaling. Clim Dyn 54(9):4309–4330. https://doi.org/10.1007/s00382-020-05231-4
6. Barrett BS, Carrasco JF, Testino AP (2012) Madden–Julian oscillation (MJO) modulation of atmospheric circulation and Chilean winter precipitation. J Clim 25(5):1678–1688. https://doi.org/10.1175/JCLI-D-11-00216.1
7. Barrett BS, Garreaud R, Falvey M (2009) Effect of the Andes Cordillera on precipitation from a midlatitude cold front. Mon Weather Rev 137(9):3092–3109. https://doi.org/10.1175/2009MWR2881.1
8. Barrett BS, Campos DA, Veloso J, Vicencio, Rondanelli R (2016) Extreme temperature and precipitation events in March 2015 in central and northern Chile. J Geophys Res Atmos 121:4563–4580. https://doi.org/10.1002/2016JD024835
9. Beck HE, Wood EF, McVicar TR, Zambrano-Bigiarini M, Alvarez-Garreton C, Baez-Villanueva OM, …, Karger DN (2020) Bias correction of global high-resolution precipitation climatologies using streamflow observations from 9372 catchments. J Clim 33(4):1299–1315. https://doi.org/10.1175/JCLI-D-19-0332.1
10. Boisier JP, Rondanelli R, Garreaud RD, Muñoz F (2016) Anthropogenic and natural contributions to the Southeast Pacific precipitation decline and recent megadrought in central Chile. Geophys Res Lett 43(1):413–421. https://doi.org/10.1002/2015GL067265
11. Boisier JP, Alvarez-Garreton C, Cordero RR, Damiani A, Gallardo L, Garreaud RD, …, Rondanelli R (2018) Anthropogenic drying in central-southern Chile evidenced by long-term observations and climate model simulations. *Elementa: Science of the Anthropocene*, *6*. https://doi.org/10.1525/elementa.328
12. Boogaard H, Schubert J, De Wit A, Lazebnik J, Hutjes R, Van der Grijn G (2020) : Agrometeorological indicators from 1979 to present derived from reanalysis, version 1.0. Copernicus Climate Change

Service (C3S) Climate Data Store (CDS), (Accessed on 10-january-2022), https://10.24381/cds.6c68c9bb

13. Bozkurt D, Rondanelli R, Garreaud R, Arriagada A (2016) Impact of warmer eastern tropical Pacific SST on the March 2015 Atacama floods. Mon Weather Rev 144(11):4441–4460. https://doi.org/10.1175/MWR-D-16-0041.1
14. Bozkurt D, Rojas M, Boisier JP, Valdivieso J (2018) Projected hydroclimate changes over Andean basins in central Chile from downscaled CMIP5 models under the low and high emission scenarios. Clim Change 150(3):131–147. https://doi.org/10.1175/MWR-D-16-0041.1
15. Burger F, Brock B, Montecinos A (2018) Seasonal and elevational contrasts in temperature trends in Central Chile between 1979 and 2015. Glob Planet Change 162:136–147. https://doi.org/10.1016/j.gloplacha.2018.01.005
16. Burkey J (2021) Mann-Kendall Tau-b with Sen's Method (enhanced) (https://www.mathworks.com/matlabcentral/fileexchange/11190-mann-kendall-tau-b-with-sen-s-method-enhanced), MATLAB Central File Exchange. Retrieved January 26, 2021
17. Center for Climate and Resilience Research, CR2 (2020) Explorador Climático. url: https://explorador.cr2.cl/
18. Cerón WL, Kayano MT, Andreoli RV, Avila-Diaz A, Ayes I, Freitas ED, …, Souza RA (2021) Recent intensification of extreme precipitation events in the La Plata Basin in Southern South America (1981–2018). Atmos Res 249:105299. https://doi.org/10.1016/j.atmosres.2020.105299
19. Cerón WL, Andreoli RV, Kayano MT, Canchala T, Ocampo-Marulanda C, Avila-Diaz A, Antunes J (2022) Trend Pattern of Heavy and Intense Rainfall Events in Colombia from 1981–2018: A Trend-EOF Approach. Atmosphere 13:156. https://doi.org/10.3390/atmos13020156
20. Chemke R, Ming Y, Yuval J (2022) The intensification of winter mid-latitude storm tracks in the Southern Hemisphere. Nat Clim Change 1–5. https://doi.org/10.1038/s41558-022-01368-8
21. Chimborazo O, Minder JR, Vuille M (2022) Observations and Simulated Mechanisms of Elevation-Dependent Warming over the Tropical Andes. J Clim 35(3):1021–1044. https://doi.org/10.1175/JCLI-D-21-0379.1
22. Elliott WP, Gaffen DJ (1991) On the utility of radiosonde humidity archives for climate studies. Bull Am Meteorol Soc 72(10):1507–1520. https://doi.org/10.1175/1520-0477(1991)072<1507:OTUORH>2.0.CO;2
23. Falvey M, Garreaud R (2007) Wintertime precipitation episodes in central Chile: Associated meteorological conditions and orographic influences. J Hydrometeorol 8(2):171–193. https://doi.org/10.1175/JHM562.1
24. Falvey M, Garreaud RD (2009) Regional cooling in a warming world: Recent temperature trends in the southeast Pacific and along the west coast of subtropical South America (1979–2006). J Geophys Research: Atmos 114(D4). https://doi.org/10.1029/2008JD010519
25. Fischer EM, Knutti R (2016) Observed heavy precipitation increase confirms theory and early models. Nat Clim Change 6(11):986–991. https://doi.org/10.1038/nclimate3110

26. Fowler HJ et al (2021) Anthropogenic intensification of short-duration rainfall extremes. Nat Reviews Earth Environ 2(2):107–122. https://doi.org/10.1038/s43017-020-00128-6
27. Funk C et al (2015) The climate hazards infrared precipitation with stations—a new environmental record for monitoring extremes. Sci data 2(1):1–21. https://doi.org/10.1038/sdata.2015.66
28. Garreaud RD, Boisier JP, Rondanelli R, Montecinos A, Sepúlveda HH, Veloso-Aguila D (2020) The central Chile mega drought (2010–2018): a climate dynamics perspective. Int J Climatol 40(1):421–439. https://doi.org/10.1002/joc.6219
29. Garreaud R, Aceituno P (2001) Interannual rainfall variability over the South American Altiplano. J Clim 14(12):2779–2789. https://doi.org/10.1175/1520-0442(2001)014<2779:IRVOTS>2.0.CO;2
30. Garreaud R (2000) Intraseasonal variability of moisture and rainfall over the South American Altiplano. Mon Weather Rev 128(9):3337–3346. https://doi.org/10.1175/1520-0493(2000)128<3337:IVOMAR>2.0.CO;2
31. Garreaud R, Falvey M, Montecinos A (2016) Orographic precipitation in coastal southern Chile: Mean distribution, temporal variability, and linear contribution. J Hydrometeorol 17(4):1185–1202. https://doi.org/10.1175/JHM-D-15-0170.1
32. Garreaud RD, Clem K, José VV (2021) The South Pacific Pressure Trend Dipole and the Southern Blob. J Clim 34:7661–7676. https://doi.org/10.1175/JCLI-D-20-0886.1
33. Guan B, Waliser DE (2015) Detection of atmospheric rivers: Evaluation and application of an algorithm for global studies. J Geophys Res Atmos 120:12514–12535. https://doi.org/10.1002/2015JD024257
34. Guerreiro SB, Fowler HJ, Barbero R, Westra S, Lenderink G, Blenkinsop S, …, Li XF (2018) Detection of continental-scale intensification of hourly rainfall extremes. Nat Clim Change 8(9):803–807. https://doi.org/10.1038/s41558-018-0245-3
35. Hardwick Jones, Rhys SW, Sharma A (2010) Observed relationships between extreme sub-daily precipitation, surface temperature, and relative humidity. Geophys Res Lett 3722. https://doi.org/10.1029/2010GL045081
36. Hersbach H, Bell B, Berrisford P, Hirahara S, Horányi A, Muñoz-Sabater J, …, Thépaut JN (2020) The ERA5 global reanalysis. Q J R Meteorol Soc 146(730):1999–2049. https://doi.org/10.1002/qj.3803
37. Hu Y, Fu Q (2007) Observed poleward expansion of the Hadley circulation since 1979. Atmos Chem Phys 7(19):5229–5236. https://doi.org/10.5194/acp-7-5229-2007
38. Hu Y, Zhou C, Liu J (2011) Observational evidence for poleward expansion of the Hadley circulation. Adv Atmos Sci 28(1):33–44. https://doi.org/10.1007/s00376-010-0032-1
39. Huang B, Thorne PW, Banzon VF, Boyer T, Chepurin G, Lawrimore JH, …, Zhang HM (2017) NOAA extended reconstructed sea surface temperature (ERSST), version 5 [1979–2017]. NOAA Natl Centers Environ Inform 30:8179–8205 [access date 02/2022]
40. Janssen E, Wuebbles DJ, Kunkel KE, Olsen SC, Goodman A (2014) Observational and model-based trends and projections of extreme precipitation over the contiguous United States. Earths Future 2(2):99–113. https://doi.org/10.1002/2013EF000185

41. Juliá C, Rahn DA, Rutllant JA (2012) Assessing the influence of the MJO on strong precipitation events in subtropical, semi-arid north-central Chile (30 S). J Clim 25:7003–7013. https://doi.org/10.1175/JCLI-D-11-00679.1
42. Kendall MG (1948) Rank correlation methods. Griffin
43. Karl TR, Nicholls N, Ghazi A (1999) Clivar/GCOS/WMO workshop on indices and indicators for climate extremes workshop summary. Weather and climate extremes. Springer, Dordrecht, pp 3–7. https://doi.org/10.1007/978-94-015-9265-9_2
44. Lagos-Zúñiga M, Vargas-Mesa X (2014) Potential Influences of Climate Change on Pluvial Floods in an Andean Watershed (in spanish). Tecnología y ciencias del agua 5(2):19–38
45. Lagos-Zúñiga M, Balmaceda-Huarte R, Regoto P, Torrez L, Olmo M, Lyra A, …, Bettolli ML (2022) Extreme indices of temperature and precipitation in South America: trends and intercomparison of regional climate models. Clim Dyn 1–22. https://doi.org/10.1007/s00382-022-06598-2
46. Lenderink G, Mok HY, Lee TC, Van Oldenborgh GJ (2011) Scaling and trends of hourly precipitation extremes in two different climate zones–Hong Kong and the Netherlands. Hydrol Earth Syst Sci 15(9):3033–3041. https://doi.org/10.5194/hess-15-3033-2011
47. Lenderink G, Barbero R, Loriaux JM, Fowler HJ (2017) Super-Clausius–Clapeyron scaling of extreme hourly convective precipitation and its relation to large-scale atmospheric conditions. J Clim 30(15):6037–6052. https://doi.org/10.1175/JCLI-D-16-0808.1
48. Loriaux JM, Lenderink G, De Roode SR, Siebesma AP (2013) Understanding convective extreme precipitation scaling using observations and an entraining plume model. J Atmos Sci 70(11):3641–3655. https://doi.org/10.1175/JAS-D-12-0317.1
49. Ma W, Chen G, Guan B (2020) Poleward shift of atmospheric rivers in the Southern Hemisphere in recent decades. Geophys Res Lett 47(21). https://doi.org/10.1029/2020GL089934. e2020GL089934
50. May RM, Arms SC, Marsh P, Bruning E, Leeman JR, Goebbert K, Thielen JE, Bruick Z, Camron MD, 2021: MetPy: A Python Package for Meteorological Data., Unidata https://github.com/Unidata/MetPy, doi:10.5065/D6WW7G29
51. Mann HB (1945) Nonparametric tests against trend. Econometrica: J econometric Soc, 245–259
52. Mardones P, Garreaud RD (2020) Future changes in the free tropospheric freezing level and rain–snow limit: The case of central Chile. Atmosphere 11(11):1259. https://doi.org/10.3390/atmos11111259
53. Martel JL, Brissette FP, Lucas-Picher P, Troin M, Arsenault R (2021) Climate Change and Rainfall Intensity–Duration–Frequency Curves: Overview of Science and Guidelines for Adaptation. J Hydrol Eng 26(10):03121001. https://doi.org/10.1061/(ASCE)HE.1943-5584.0002122
54. Martel J-L et al (2018) Role of natural climate variability in the detection of anthropogenic climate change signal for mean and extreme precipitation at local and regional scales. J Clim 31:4241–4263. https://doi.org/10.1175/JCLI-D-17-0282.1
55. Martinkova M, Kysely J (2020) Overview of observed Clausius-Clapeyron scaling of extreme precipitation in midlatitudes. Atmosphere 11(8):786. https://doi.org/10.3390/atmos11080786

56. Molnar P, Fatichi S, Gaál L, Szolgay J, Burlando P (2015) Storm type effects on super Clausius–Clapeyron scaling of intense rainstorm properties with air temperature. Hydrol Earth Syst Sci 19(4):1753–1766. https://doi.org/10.5194/hess-19-1753-2015
57. Mukherjee S et al (2018) Increase in extreme precipitation events under anthropogenic warming in India. Weather and climate extremes 20:45–53. https://doi.org/10.1016/j.wace.2018.03.005
58. Muñoz C, Schultz DM (2021) Cutoff Lows, Moisture Plumes, and Their Influence on Extreme-Precipitation Days in Central Chile. J Appl Meteorol Climatology 60(4):437–454. https://doi.org/10.1175/JAMC-D-20-0135.1
59. Ortega C, Vargas G, Rojas M, Rutllant JA, Muñoz P, Lange CB, …, Ortlieb L (2019) Extreme ENSO-driven torrential rainfalls at the southern edge of the Atacama Desert during the Late Holocene and their projection into the 21th century. Glob Planet Change 175:226–237. https://doi.org/10.1016/j.gloplacha.2019.02.011
60. Pal I, Al-Tabbaa A (2009) Trends in seasonal precipitation extremes–An indicator of 'climate change' in Kerala, India. J Hydrol 367(1–2):62–69. https://doi.org/10.1016/j.jhydrol.2008.12.025
61. Paxian A, Hertig E, Seubert S, Vogt G, Jacobeit J, Paeth H (2015) Present-day and future Mediterranean precipitation extremes assessed by different statistical approaches. Clim Dyn 44(3):845–860. https://doi.org/10.1007/s00382-014-2428-6
62. Pei F et al (2018) "Detection and attribution of extreme precipitation changes from 1961 to 2012 in the Yangtze River Delta in China." *Catena* 169 : 183–194. https://doi.org/10.1016/j.catena.2018.05.038
63. Pepin NC, Lundquist JD (2008) Temperature trends at high elevations: patterns across the globe. Geophys Res Lett 35(14). https://doi.org/10.1029/2008GL034026
64. Pepin N, Bradley RS, Diaz HF, Baraer M, Caceres EB, Forsythe N, …, Yang DQ (2015) Elevation-dependent warming in mountain regions of the world. Nat Clim Change 5:424–430. https://doi.org/10.1038/nclimate2563
65. Pepin NC, Arnone E, Gobiet A, Haslinger K, Kotlarski S, Notarnicola C, …, Adler C (2022) Climate changes and their elevational patterns in the mountains of the world. Rev Geophys 60(1). https://doi.org/10.1029/2020RG000730. e2020RG000730
66. Prein AF, Mearns LO (2021) US extreme precipitation weather types increased in frequency during the 20th century. *Journal of Geophysical Research: Atmospheres*, *126*(7), e2020JD034287. https://doi.org/10.1029/2020JD034287
67. Regoto P, Dereczynski C, Chou SC, Bazzanela AC (2021) Observed changes in air temperature and precipitation extremes over Brazil. Int J Climatol. https://doi.org/10.1002/joc.7119
68. Rondanelli R, Hatchett B, Rutllant J, Bozkurt D, Garreaud R (2019) Strongest MJO on record triggers extreme Atacama rainfall and warmth in Antarctica. Geophys Res Lett 46(6):3482–3491. https://doi.org/10.1029/2018GL081475
69. Ross RJ, Gaffen DJ (1998) Comment on "Widespread tropical atmospheric drying from 1979 to 1995" by Schroeder and McGuirk. Geophys Res Lett 25(23):4357–4358.

https://doi.org/10.1029/1998GL900169

70. Rutllant J, Matus F, Rudloff V, Rondanelli R (2023) The role of atmospheric rivers in rainfall-induced landslides: A study from the Elqui valley, J Arid Environ.
71. Saavedra FA, Kampf SK, Fassnacht SR, Sibold JS (2018) Changes in Andes snow cover from MODIS data, 2000–2016. The Cryosphere 12(3):1027–1046. https://doi.org/10.5194/tc-12-1027-2018
72. Sarricolea P, Herrera-Ossandon M, Meseguer-Ruiz Ó (2017) Climatic regionalization of continental Chile. J Maps 13(2):66–73. https://doi.org/10.1080/17445647.2016.1259592
73. Sarricolea P et al (2019) "Trends of daily precipitation concentration in Central-Southern Chile." *Atmospheric research* 215 : 85–98. https://doi.org/10.1016/j.atmosres.2018.09.005
74. Scaff L, Rutllant JA, Rahn D, Gascoin S, Rondanelli R (2017) Meteorological interpretation of orographic precipitation gradients along an Andes west slope basin at 30 S (Elqui Valley, Chile). J Hydrometeorol 18(3):713–727. https://doi.org/10.1175/JHM-D-16-0073.1
75. Schumacher V, Justino F, Fernández A, Meseguer-Ruiz O, Sarricolea P, Comin A, …, Althoff D (2020) Comparison between observations and gridded data sets over complex terrain in the Chilean Andes: Precipitation and temperature. Int J Climatol 40(12):5266–5288. https://doi.org/10.1002/joc.6518
76. Sen PK (1968) Estimates of the regression coefficient based on Kendall's tau. J Am Stat Assoc 63(324):1379–1389. https://doi.org/10.2307/2285891
77. Shaw T, Baldwin M, Barnes E et al (2016) Storm track processes and the opposing influences of climate change. Nat Geosci 9:656–664. https://doi.org/10.1038/ngeo2783
78. Shi J, Cui L, Wang J, Du H, Wen K (2019) Changes in the temperature and precipitation extremes in China during 1961–2015. Quatern Int 527:64–78. https://doi.org/10.1016/j.quaint.2018.08.008
79. Somos-Valenzuela MA, Oyarzún-Ulloa JE, Fustos-Toribio IJ, Garrido-Urzua N, Chen N (2020) The mudflow disaster at Villa Santa Lucía in Chilean Patagonia: understandings and insights derived from numerical simulation and postevent field surveys. Nat Hazards Earth Syst Sci 20(8):2319–2333. https://doi.org/10.5194/nhess-20-2319-2020
80. Souvignet M, Oyarzún R, Verbist KM, Gaese H, Heinrich J (2012) Hydro-meteorological trends in semi-arid north-central Chile (29–32 S): Water resources implications for a fragile Andean region. Hydrol Sci J 57(3):479–495. https://doi.org/10.1080/02626667.2012.665607
81. Taszarek M, Allen JT, Marchio M, Brooks HE (2021) Global climatology and trends in convective environments from ERA5 and rawinsonde data. NPJ Clim atmospheric Sci 4(1):1–11. https://doi.org/10.1038/s41612-021-00190-x
82. Trenberth KE (2011) Changes in precipitation with climate change. Climate Res 47(1–2):123–138. https://doi.org/10.3354/cr00953
83. Valdes-Pineda R, Pizarro R, Valdes JB, Carrasco JF, Garcia-Chevesich P, Olivares C (2016) Spatio-temporal trends of precipitation, its aggressiveness and concentration, along the Pacific coast of South America (36–49 S). Hydrol Sci J 61(11):2110–2132. https://doi.org/10.1080/02626667.2015.1085989

84. Valenzuela R, Garreaud R, Vergara I, Campos D, Viale M, Rondanelli R (2022) An extraordinary dry season precipitation event in the subtropical Andes: Drivers, impacts and predictability. Weather and Climate Extremes 37:100472. https://doi.org/10.1016/j.wace.2022.100472
85. Valenzuela RA, Garreaud RD (2019) Extreme daily rainfall in central-southern Chile and its relationship with low-level horizontal water vapor fluxes. J Hydrometeorol 20(9):1829–1850. https://doi.org/10.1175/JHM-D-19-0036.1
86. Viale M, Nuñez MN (2011) Climatology of winter orographic precipitation over the subtropical central Andes and associated synoptic and regional characteristics. J Hydrometeorol 12(4):481–507. https://doi.org/10.1175/2010JHM1284.1
87. Viale M, Garreaud R (2014) Summer precipitation events over the western slope of the subtropical Andes. Mon Weather Rev 142(3):1074–1092. https://doi.org/10.1175/MWR-D-13-00259.1
88. Viale M, Valenzuela R, Garreaud RD, Ralph FM (2018) Impacts of atmospheric rivers on precipitation in southern South America. J Hydrometeorol 19(10):1671–1687. https://doi.org/10.1175/JHM-D-18-0006.1
89. Viale M, Bianchi E, Cara L, Ruiz LE, Villalba R, Pitte P, …, Zalazar L (2019) Contrasting climates at both sides of the Andes in Argentina and Chile. Front Environ Sci 7:69. https://doi.org/10.3389/fenvs.2019.00069
90. Vicuña S, Vargas X, Boisier JP, Mendoza PA, Gómez T, Vásquez N, Cepeda J (2021) Impacts of Climate Change on Water Resources in Chile. Water Resources of Chile. Springer, Cham, pp 347–363
91. Vicencio J, Rondanelli R, Campos D, Valenzuela R, Garreaud R, Reyes A, …, Nicora G (2021) The Chilean tornado outbreak of May 2019: synoptic, mesoscale, and historical contexts. Bull Am Meteorol Soc 102(3):E611–E634. https://doi.org/10.1175/BAMS-D-19-0218.1
92. Vuille M (1999) Atmospheric circulation over the Bolivian Altiplano during dry and wet periods and extreme phases of the Southern Oscillation. Int J Climatology: J Royal Meteorological Soc 19(14):1579–1600. https://doi.org/10.1002/(SICI)1097-0088(19991130)19:14<1579::AID-JOC441>3.0.CO;2-N
93. Wang G et al (2017) The peak structure and future changes of the relationships between extreme precipitation and temperature. Nat Clim Change 7(4):268–274. https://doi.org/10.1038/nclimate3239
94. Wilcox AC, Escauriaza C, Agredano R, Mignot E, Zuazo V, Otárola S, …, Mao L (2016) An integrated analysis of the March 2015 Atacama floods. Geophys Res Lett 43(15):8035–8043. https://doi.org/10.1002/2016GL069751
95. Wilcoxon F (1992) Individual comparisons by ranking methods. Breakthroughs in statistics. Springer, New York, NY, pp 196–202. https://doi.org/10.2307/3001968
96. Zhai P, Zhang X, Wan H, Pan X (2005) Trends in total precipitation and frequency of daily precipitation extremes over China. J Clim 18(7):1096–1108. https://doi.org/10.1175/JCLI-3318.1
97. Zolina O, Simmer C, Kapala A, Bachner S, Gulev S, Maechel H (2008) Seasonally dependent changes of precipitation extremes over Germany since 1950 from a very dense observational network. J

Geophys Research: Atmos 113(D6). https://doi.org/10.1029/2007JD008393

98. Zou S et al (2021) "Attribution of changes in the trend and temporal non-uniformity of extreme precipitation events in Central Asia." *Scientific reports* 11.1 : 1–11. https://doi.org/10.1038/s41598-021-94486-w

Figures

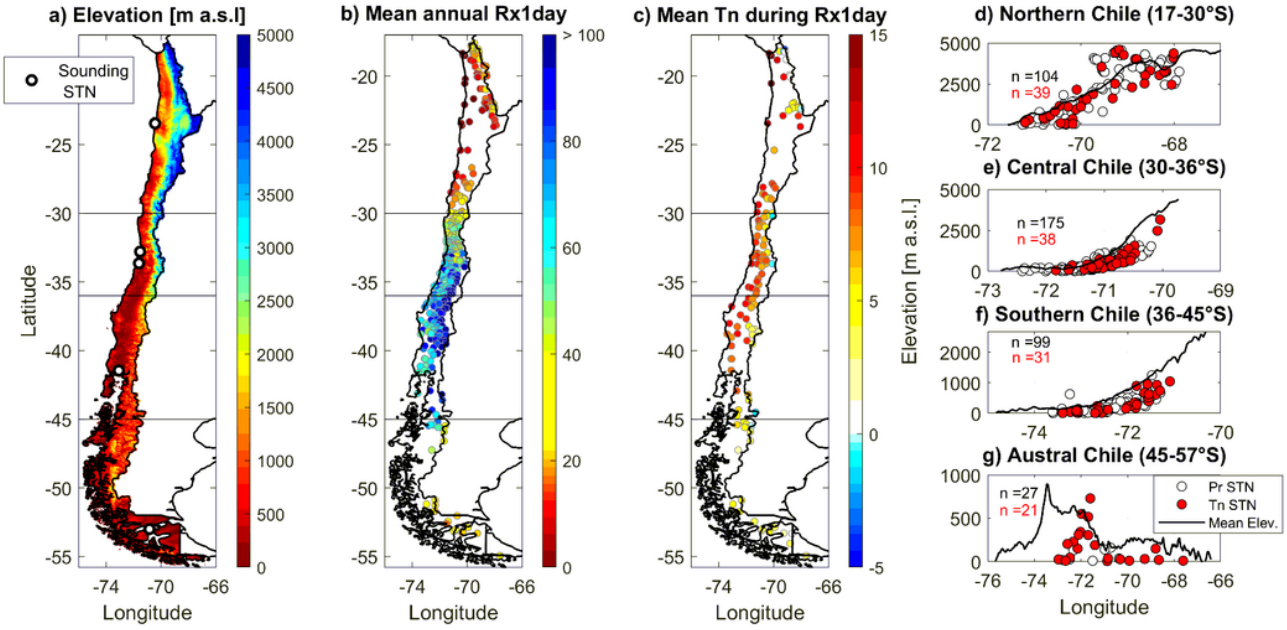

Figure 1

a) Elevation of continental Chile and location of the five radiosonde stations, b) mean annual Rx1day, c) mean Tn during mean annual Rx1day, d)-g) mean longitudinal elevation by region, Pr stations (white circles), and Tn/Tx stations (red circles). The horizontal lines in panels a)-c) represent the limits between Northern (15-30°S), Central (30-36°S), Southern (36-45°S), and Austral (45-57°S) Chile.

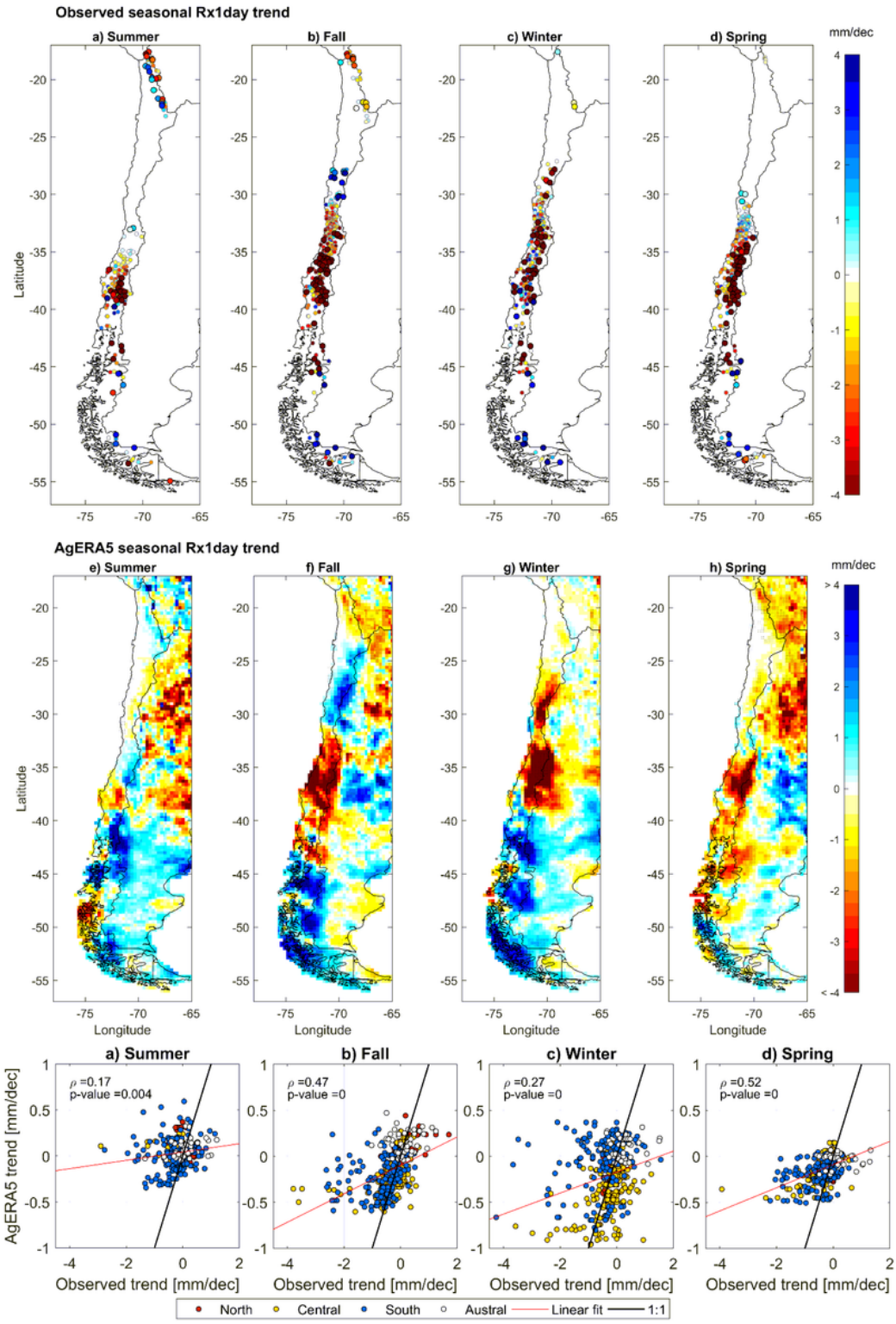

Figure 2

Sen's slope for (a-d) observed and (e-h) AgERA5 trends in seasonal Rx1day; and (i-l) relationship between AgERA5 and observed trends (1979-2017). The results are stratified for (a,e, i) summer (DJF), (b,f,j) fall (MAM), (c,g,k) winter (JJA), and (d,h, l) spring (SON). Larger circles (a-d) and dotted surfaces (e-h) denote statistically significant trends at a 90% confidence level.

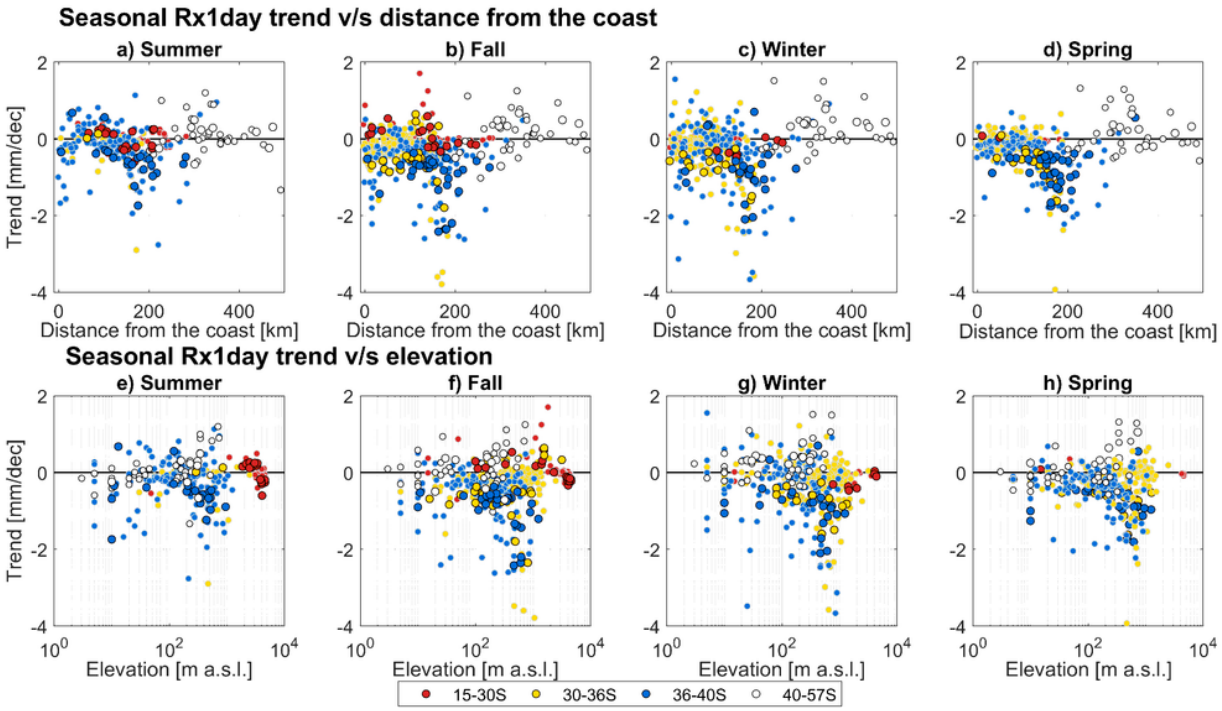

Figure 3

Sen's slopes for seasonal Rx1day as a function of distance from the coast and elevation for meteorological stations across different Chilean regions and seasons. Stations with non-significant trends or < 25 years of records are displayed in smaller circles. The number of stations in each panel is shown in Table S1.

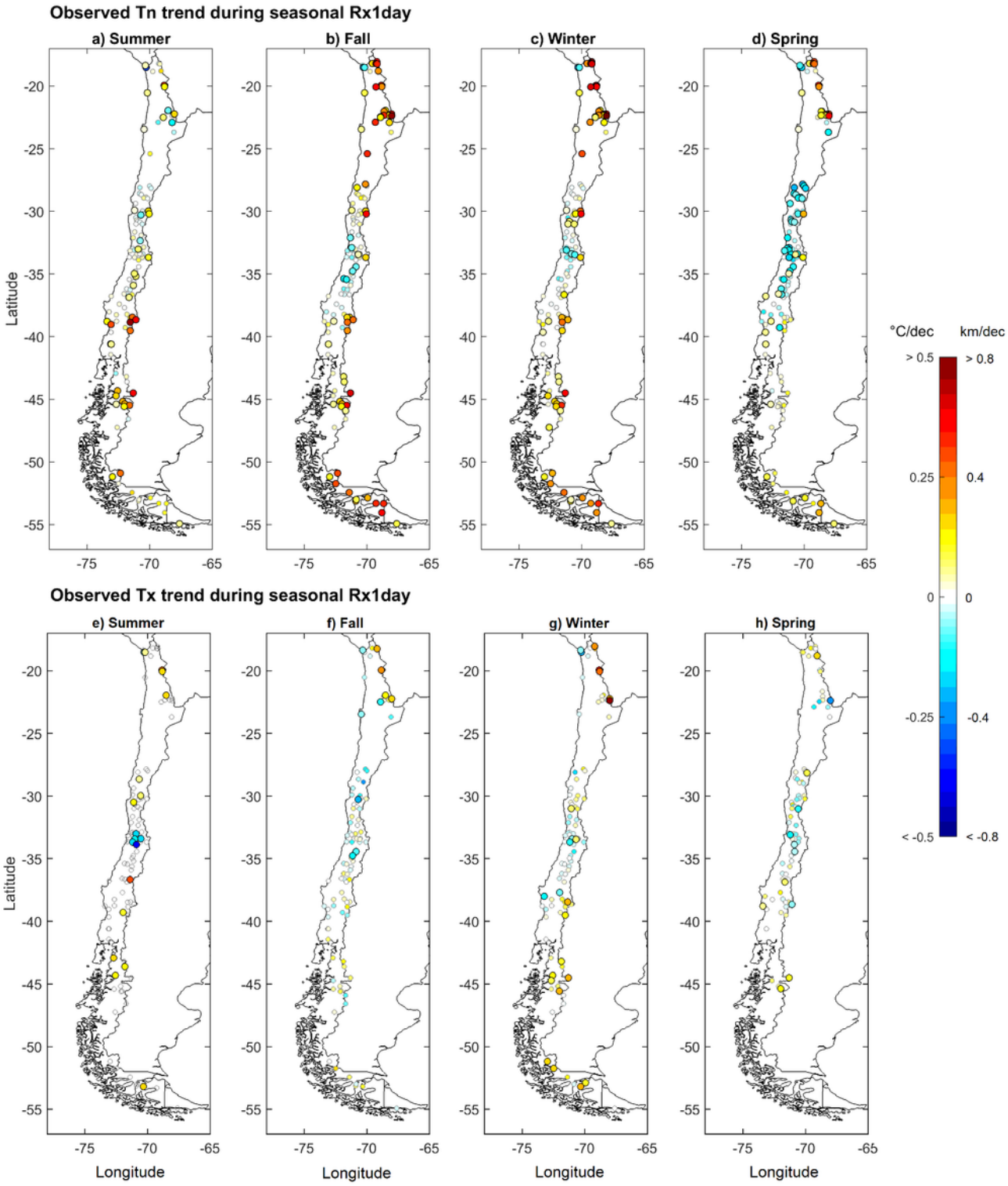

Figure 4

Same as in Figure 2, but for Tn (up) and Tx (down) during seasonal Rx1day.

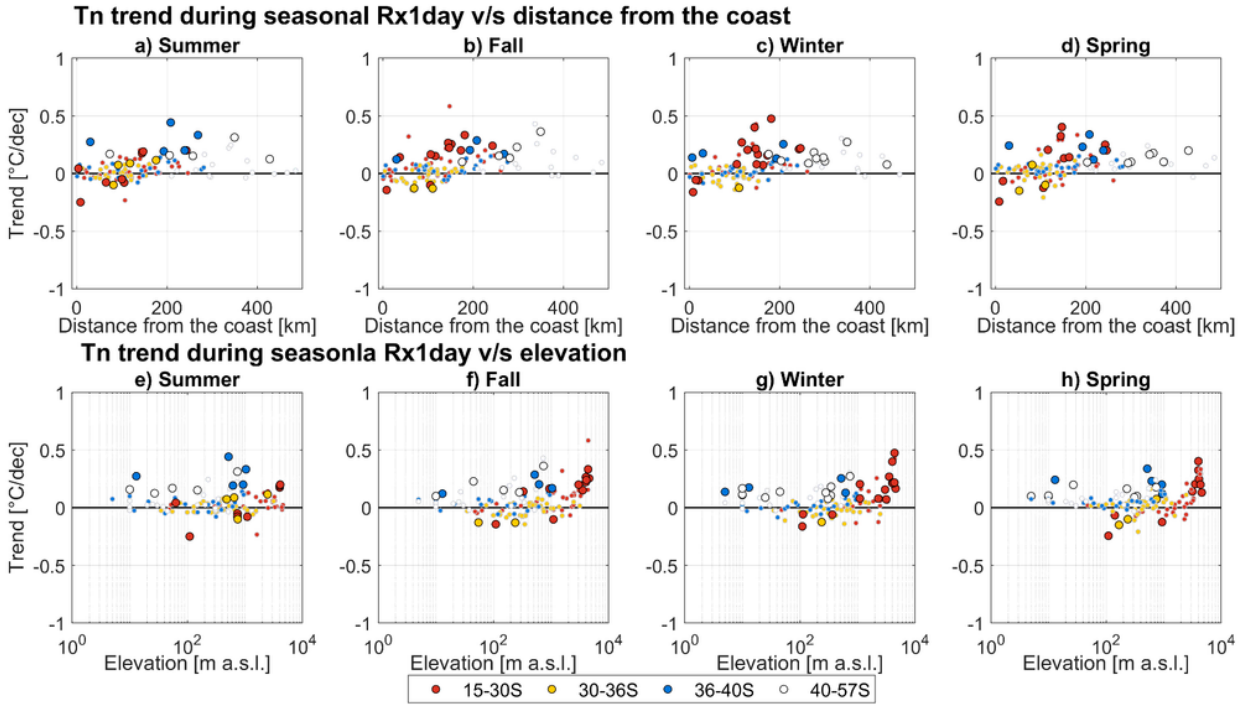

Figure 5

Same as in Figure 3, but for Tn during seasonal RX1day. The number of stations in each panel is shown in Table S2.

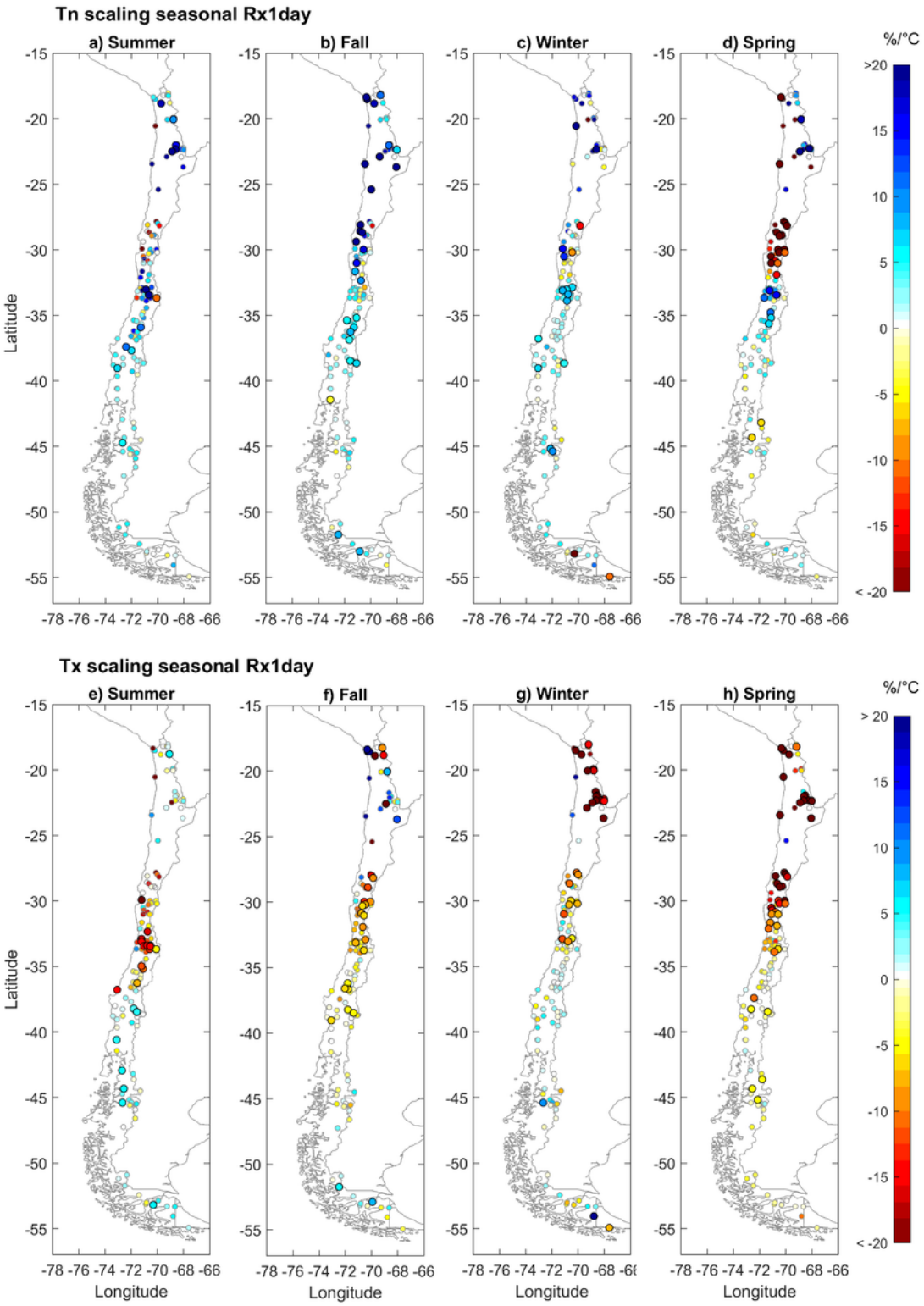

Figure 6

Sensitivities of seasonal Rx1day to Tn variations from 1979 to 2017.

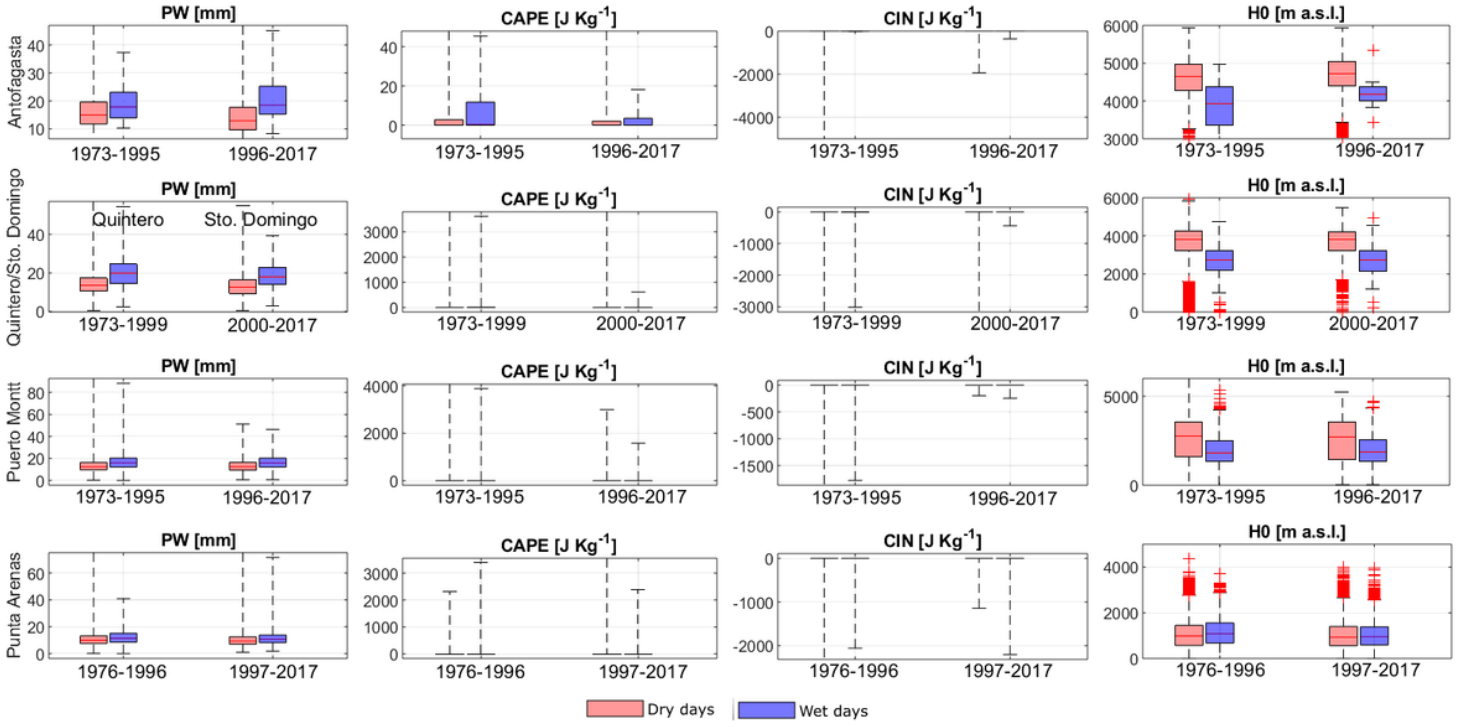

Figure 7

Comparison of daily observations of PW (mm), CAPE (J kg-1), CIN (J kg-1), and H0 (m a.s.l.) obtained from sounding observations during dry and wet days in two periods.

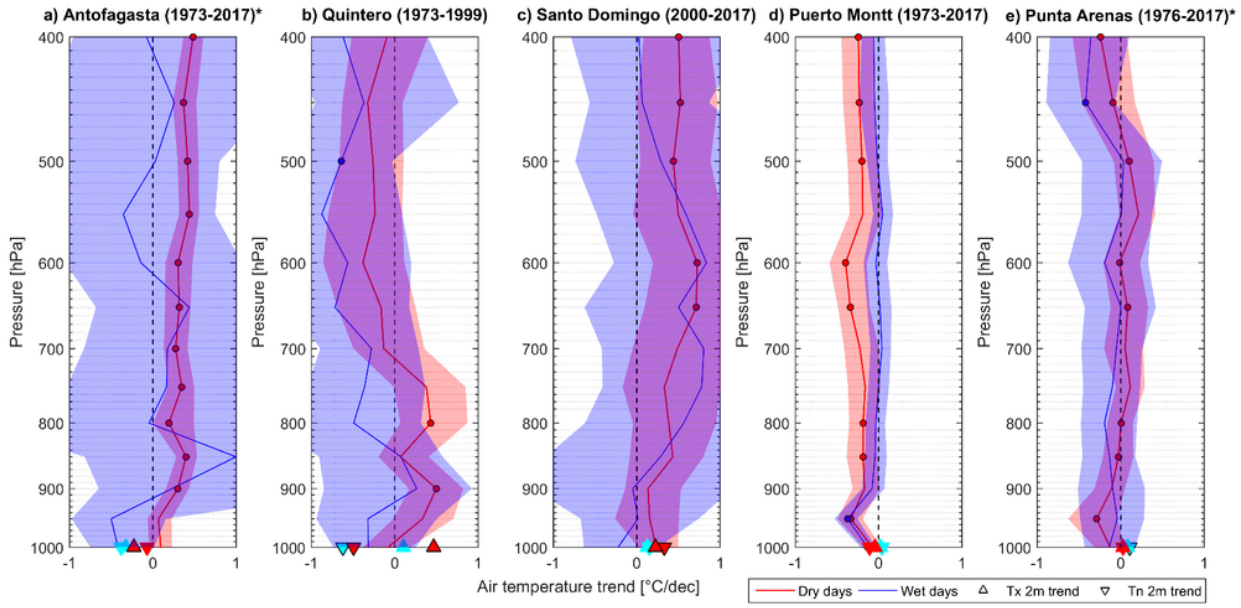

Figure 8

Air temperature trends (°C/dec) for radiosonde stations during wet (blue) and dry (red) days. (*) stands for fewer yearly available records than other stations (Figure S6). Cyan triangles: wet days, red triangles:

dry days, circles, and black-contoured markers indicate statistically significant trends. Shaded areas show the 90% confidence intervals for the sounding trends.

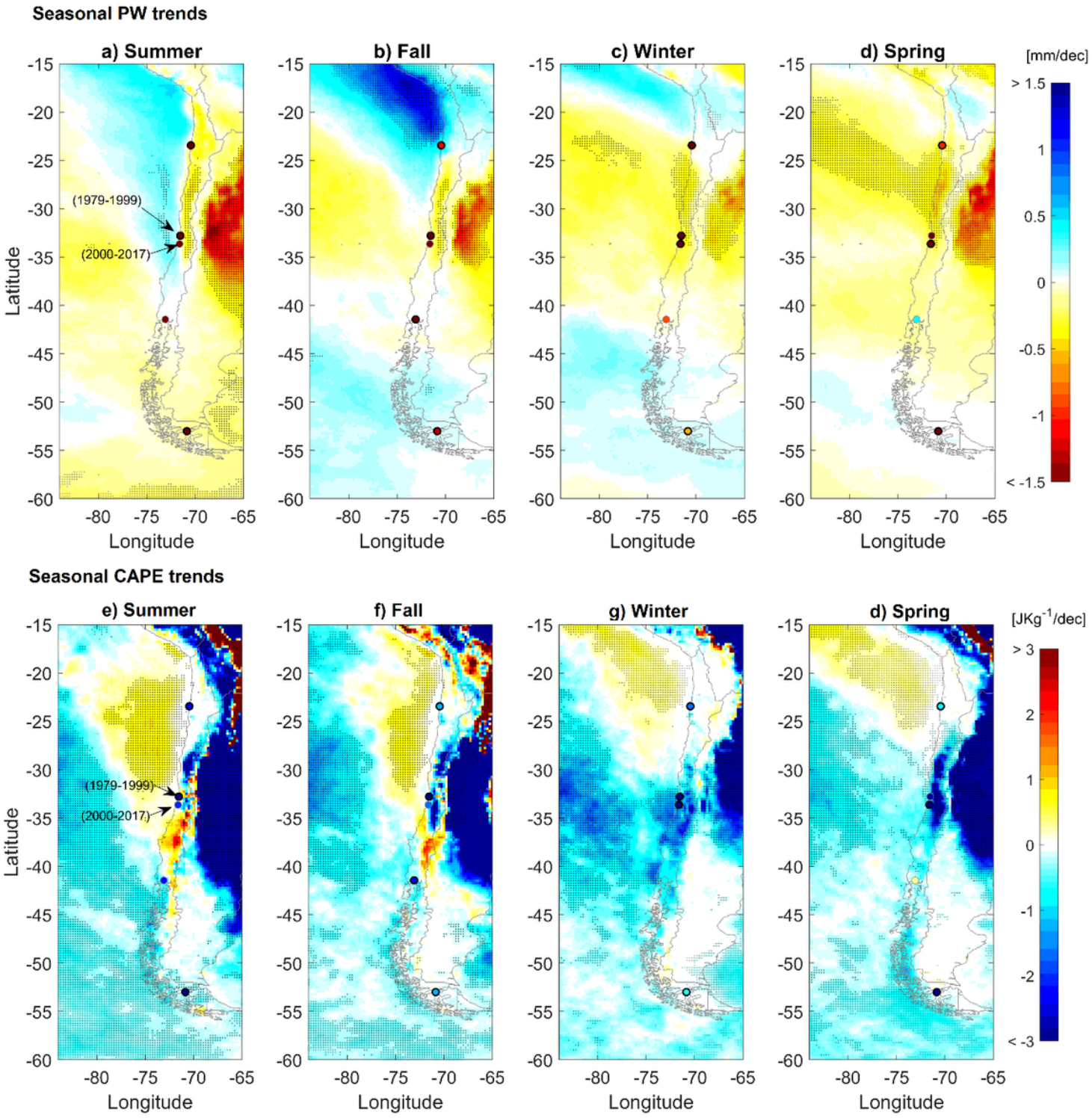

Figure 9

(a-d) Trends for seasonal precipitable water [mm/dec] (e-h) Trends for CAPE [JKg-1/dec] retrieved from monthly averaged ERA5 reanalysis for the 1979-2017 period. Shadowed surfaces denote statistically

significant trends. Sounding station trends are shown in circles, and the black-contoured circles stand for statistically significant trends.

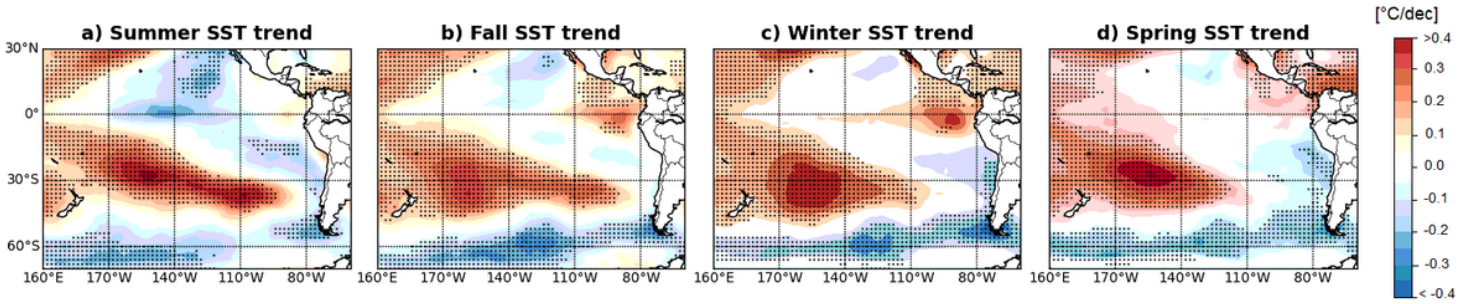

Figure 10

Seasonal SST trends (1979-2017). Circles denote statistically significant trends.

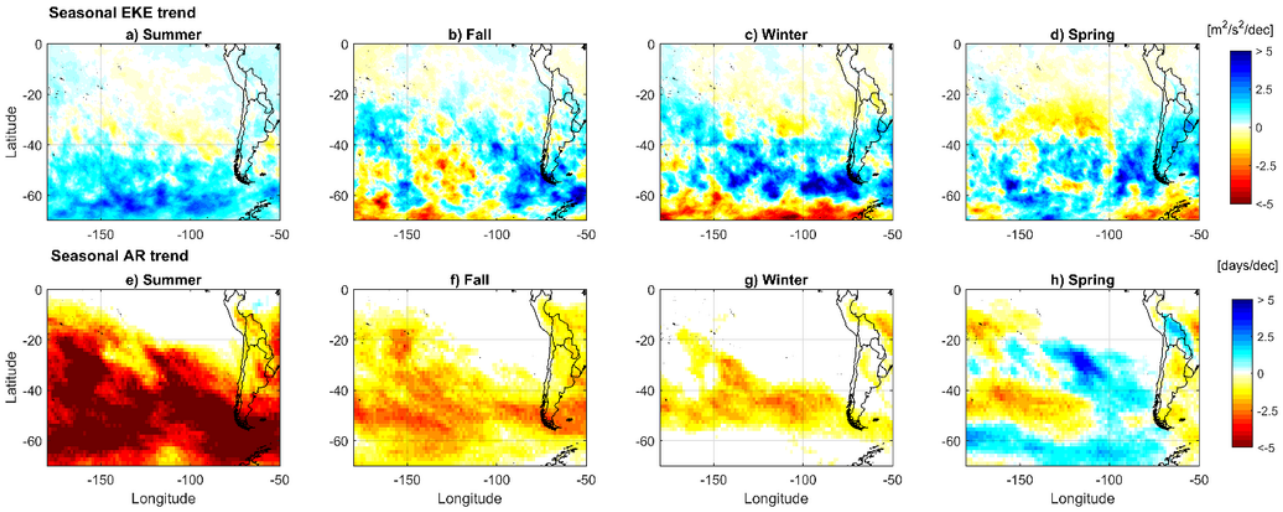

Figure 11

(a-d): Seasonal EKE trends (1979-2014) retrieved from ERA5 reanalysis; (e-h) seasonal AR trends (1979-2014) retrieved from Guan and Waliser (2015).

Supplementary Files

This is a list of supplementary files associated with this preprint. Click to download.

- renamed96b19.docx